

Homologous large-scale activity in solar eruptive events of 24–26 November 2000

I. M. Chertok,¹ V. V. Grechnev,² H. S. Hudson,³ and N. V. Nitta⁴

Received 5 August 2003; revised 15 October 2003; accepted 23 October 2003; published 21 February 2004.

[1] We study large-scale activity on the solar disk associated with a 24–26 November 2000 series of six recurrent major flares and “halo” coronal mass ejections (CMEs). The analysis is based mainly on the SOHO/EIT data, particularly by using properly rotated difference full-disk images with 12-min intervals at 195 Å as well as with 6-hour intervals at 171, 195, 284, and 304 Å. We demonstrate that these eruptive events were homologous not only by their flare and CME characteristics, as *Nitta and Hudson* [2001] showed, but also in terms of their large-scale CME-associated manifestations in the EUV corona. These include long and narrow channeled dimmings, some transequatorial; anisotropic coronal waves, propagating in a restricted angular sector; and additional quasi-stationary emitting fronts. As a whole, in all of these six events, the homologous CME-associated disturbances covered a considerable portion of the solar disk. The homology tendency appears to be due to significant disturbance, partial eruption, and relatively fast restoration of the same large-scale structures involved in the repeating CME events. We briefly discuss the implications of the analysis in connection with the nature of coronal equilibrium.

INDEX TERMS: 7509 Solar Physics, Astrophysics, and Astronomy: Corona; 7519 Solar Physics, Astrophysics, and Astronomy: Flares; 7513 Solar Physics, Astrophysics, and Astronomy: Coronal mass ejections; 7524 Solar Physics, Astrophysics, and Astronomy: Magnetic fields; 7537 Solar Physics, Astrophysics, and Astronomy: Solar and stellar variability; *KEYWORDS:* corona, magnetic fields, flares, coronal mass ejections, homology

Citation: Chertok, I. M., V. V. Grechnev, H. S. Hudson, and N. V. Nitta (2004), Homologous large-scale activity in solar eruptive events of 24–26 November 2000, *J. Geophys. Res.*, 109, A02112, doi:10.1029/2003JA010182.

1. Introduction

[2] An outstanding series of recurrent powerful flares and large eruptive events occurred during a 2.5-day period of 24–26 November 2000 initiated by the activity in the one active region (AR) 9236 located in the northern hemisphere near and westward of the central meridian (Solar-Geophysical Data, No. 681, part II, 2001). In particular, the series included five X-class and one M3.5-class flares, recorded with the GOES soft X-ray detector, and associated “halo” coronal mass ejections (CMEs) [Howard *et al.*, 1982] observed with the Large Angle Spectroscopic Coronagraph (LASCO) [Brueckner *et al.*, 1995] on the Solar and Heliospheric Observatory (SOHO) [Domingo *et al.*, 1995].

[3] *Nitta and Hudson* [2001, hereinafter referred to as Paper I] outlined the general characteristics of these events, studying mainly the small-scale local activity within the limits of the AR. They noted that the major flares were not

long-decay events (LDEs) [Kahler, 1977] in terms of soft X-ray light curves and morphologies. They further concluded, based on magnetograms gathered with the Michelson-Doppler Imager (MDI) [Scherrer *et al.*, 1995] on SOHO, that the origin and related formation of the CMEs were caused by continual restructuring of small-scale magnetic fields due to flux emergence around the preceding spot. This flux emergence appeared to lead to the homology of the events, which was pronounced in some cases; note however that the flare location shifted to the south in the events they listed as *e* and *f*, reflecting the evolving pattern of flux emergence. Continuing flux emergence is often cited as a cause of homologous flaring [e.g., Ranns *et al.*, 2000]. Additional information on one of the events of Paper I appears in the work of Wang *et al.* [2002].

[4] In this paper, we extend the analysis of Paper I and concentrate on large-scale manifestations of the same eruptive events on spatial scales much larger than the size of the AR. In particular, based on data of the SOHO Extreme ultraviolet Imaging Telescope (EIT) [Delaboudinière *et al.*, 1995], we have formed full-disk difference images with 12-min cadence at 195 Å and with 6-hour cadence at all four EIT passbands (171, 195, 284, 304 Å). The detailed 195 Å data reveal such typical CME-associated large-scale phenomena as extended dimmings (i.e., transient areas of reduced intensity) and coronal waves (bright propagating or quasi-stationary fronts) [e.g., Hudson and Webb, 1997;

¹Solar Physics Division, Institute of Terrestrial Magnetism, Ionosphere and Radiowave Propagation (IZMIRAN), Troitsk, Russia.

²Institute of Solar-Terrestrial Physics, Irkutsk, Russia.

³Space Sciences Laboratory, University of California, Berkeley, California, USA.

⁴Lockheed Martin Solar and Astrophysics Laboratory, Palo Alto, California, USA.

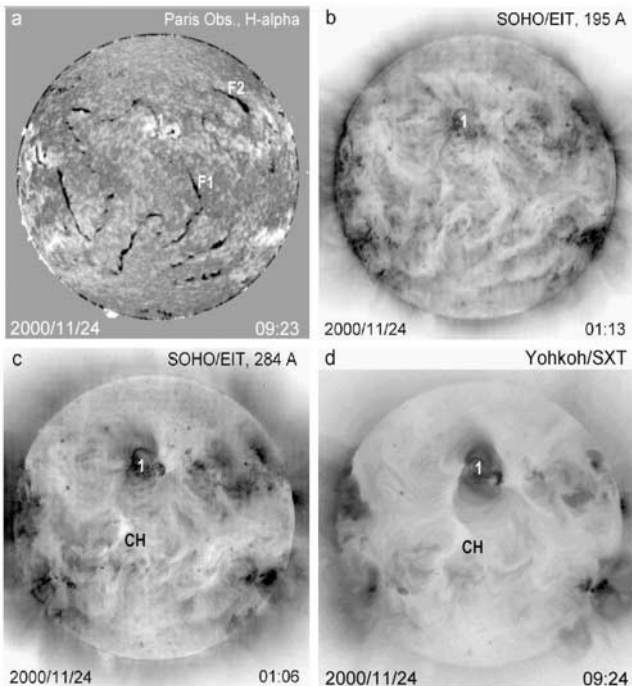


Figure 1. H α (a), EUV (b, c), and soft X-ray (d) heliograms illustrating the situation on the disk at the onset of the events under consideration. The flaring active region AR 9236 is labeled 1. A central coronal hole (CH) and optical filament (F1) as well as a northwestern filament (F2) are denoted as well. These are negative images for clarity.

[5] Let us start with some remarks concerning processing of the full-disk EIT images. As is known, such dynamic phenomena as dimmings and coronal waves are most pronounced on difference images. A realistic view of these CME-associated disturbances can be revealed by forming rotated fixed difference images. In this presentation, to avoid the appearance of false darkenings and brightenings, all disk images of the given event are rotated to a common preevent time, and then the same preevent image is subtracted from all subsequent heliograms. The image-rotation

2. Observations

[6] The running difference 12-min cadence images at 195 Å (formed by subtraction of each immediately preceding image) may produce false features when structures change their location or intensity, but they do emphasize variations occurring between adjacent images. Such running-difference images and movies are suitable for careful consideration of coronal waves and can be used as a helpful presentation in combination with rotated fixed-difference images and movies, referring to the latter to check validity.

[7] The software is fully orthographic at the photosphere, i.e., the rotation is applied to the whole visible solar hemisphere and the spherical surface at the photospheric radius is rotated. This compensation for rotation is valuable even in working with the 195 Å data at 12-min cadence because the image scale is the whole Sun. The orthographic projection is quite necessary in analysis of the 6-hour steps at 171, 284, and 304 Å [Chertok and Grechnev, 2003b]. Two kinds of errors remain. We do not know if the features rotate rigidly or differentially. We assume rigid rotation, which corresponds to a maximum possible error of about 11 arc sec over the 6-hour differences. Another source of error is the height structure of the coronal structures. It would be difficult to account for this factor in a general procedure, but the error here would not exceed 16 arc sec for coronal structures as high as 200 Mm. Neither error will substantially distort relatively large-scale features such as dimmings.

[8] The limited volume of this paper allows us to show only the most essential illustrations. Both the rotated fixed and running difference images and movies as well as some other data for all of six events under consideration are presented at the web site http://helios.izmiran.troitsk.ru/lars/Chertok/001124_26/index.html. The LASCO C2 difference pictures of the corresponding “halo” CMEs, soft and hard X-ray light curves, white-light images from the Transition Region and Coronal Explorer (TRACE) [Handy et al., 1999] and MDI magnetograms, Yohkoh flare images from Yohkoh Soft X-ray Telescope (SXT) [Tsuneta et al., 1991] and Hard X-ray Telescope (HXR) [Kosugi et al., 1991] data on variations of magnetic flux, and other illustrations can be seen in the figures of Paper I.

[9] Figure 1 of this paper shows the situation on the disk at the onset of the period of our interest as visible in H α , EUV, and soft X-ray heliograms. We consider flare events occurring in the dominant NOAA AR 9236 (hereafter region 1) located at heliographic latitude N18. As will be demonstrated below, the associated CMEs appeared to affect also an extended northward high-latitude region, ARs to the west, a large southward area including a narrow transequatorial coronal hole (CH), its outskirts, and an arcade situated over a central filament F1. Some additional but probably independent activity took place also during this period in the northeastern AR 9240 and in the southwestern quadrant. As a whole, numerous optical filaments and various structures visible in SOHO/EIT and Yohkoh/SXT coronal images testify to the presence of a complicated solar magnetosphere at this time.

[10] In order to facilitate the subsequent description and identification of the events, their labels, date, peak time in soft X-rays, flare location, and GOES class are summarized in Table 1 according to Paper 1. We however excluded Paper 1’s flare g of 25 November, 0131 UT because it took place in a different region (AR 9240).

Table 1. Positions and GOES Fluxes of Flare Events

ID	Day	Peak, UT	Longitude	GOES
a	24	0502	W05	X2.0
b	24	1513	W11	X2.3
c	24	2200	W15	X1.8
d	25	0920	W21	M3.5
e	25	1845	W24	X1.9
f	26	1648	W36	X4.0

[10] The detailed evolution of dimmings and coronal waves in each event can be seen by means of movies presented at the site mentioned above. Shown in Figure 2 is a collection of rotated fixed difference EIT images at 195 Å demonstrating the most developed stages of the CME-associated disturbances for the corresponding events *a*–*f* under consideration. Figure 2 shows that in event *a*, anisotropic dimmings are displayed as three narrow channels of a length comparable with the solar radius. Two of them, 1–2 and 1–3–4, emanate southward of AR 1, cross the equator and appear to outline footpoints of the coronal arcade existing over filament F1 (see Figure 1). The eastern dimming channel 1–2 stretches first along the western boundary of the coronal hole CH and then deviates westward. As a result, the area of the preexisting CH seems to increase temporarily due to this transient dimming. There are some dimming branches that partly mark arcade loops going from channel 1–2 to channel 1–3–4. The latter joins by a narrow fragmentary darkening 3–5 with the third similar dimming channel 5–6 arriving at northwest AR 6. A weaker dimming ribbon 7–8 is present in the northwest quadrant near filament F2 (Figure 1). Several additional relatively small dimming patches can be distinguished northward and westward of the eruptive center 1 (the active region).

[11] By the onset of event *b*, the structures that dimmed in the course of event *a* have restored their intensity. Then, as Figure 2b shows, an almost analogous system of channeled dimmings develops in event *b*. The southern branches 1–2 and 1–3–4 keep their forms, sizes, and locations. The westward dimming 3–5 and a western part of the northwest dimming ribbon 7–8 become more pronounced. However, the dimming between points 5 and 6 is not visible, and only a part of this dimming adjoining directly to region 6 is present. In return, a new but not so deep dimming ribbon 4–9 emanates from the end of channel 1–3–4 in direction to the west limb and perhaps to the southwest AR 10.

[12] Somewhat different structures of the dimmings are observed in events *c* and *d*. In the first case *c*, besides dimmings located directly nearby the eruptive center 1, only the northern part of the eastern meridian channel 1–2 persists as a branch 1–11, and a new pronounced longitudinal dimming sector 11–12 is formed in the northern segment of the preevent EUV and soft X-ray arcade (see Figure 1). This also causes a transient increase of the CH area at this place. The distinct westward disturbance zone between ARs 1 and 6 appears to be restoring its intensity after previous event *b*. For this reason, some brightenings are visible on difference images partly at the place of the former western meridional dimming channel 1–4 and some other dimmings going to outskirts of the western AR 6. Event *d* reveals a similar pronounced longitudinal dimming sector 11–12. However, in this case just a northern part 1–13 of the western meridian dimming 1–4 and fragmentary dimmings, stretching to the west limb area 5 and AR 6, are clearly visible, while a north part of the eastern meridian dimming 1–2 relaxes substantially.

[13] In the course of event *e*, the dimming structure returns to that observed in events *a* and *b* with two

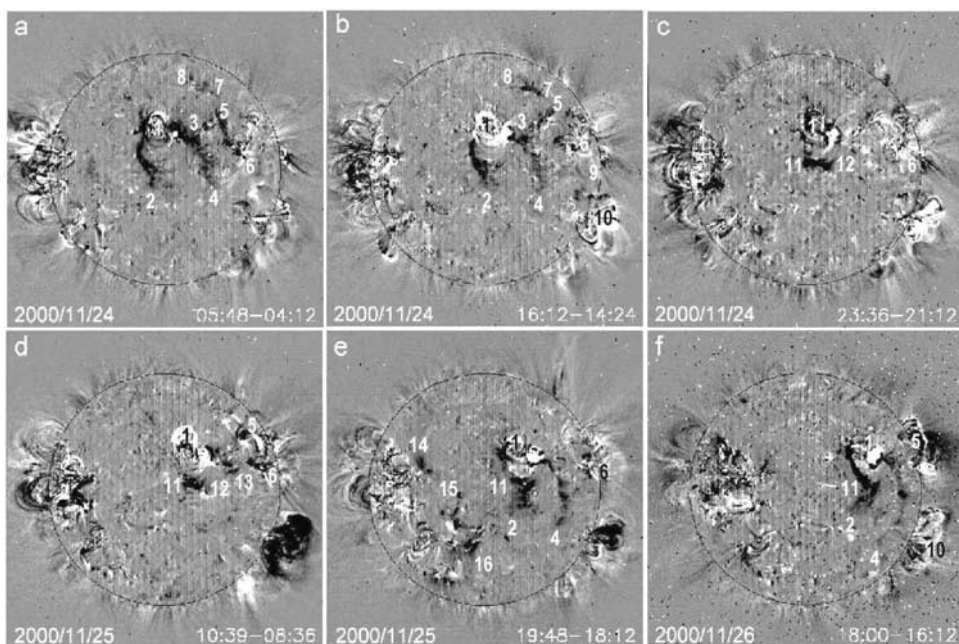


Figure 2. SOHO/EIT fixed difference full-disk images at 195 Å, made by full orthographic rotation and reprojection of the images, showing the most developed large-scale dimmings for all six events of the series. This and the following images are positive images, in the sense later minus earlier, and therefore differ from the convention in Figure 1.

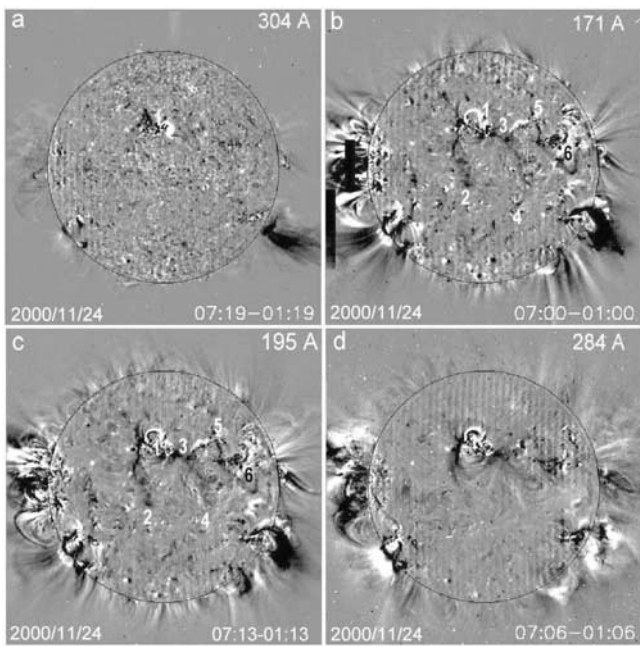


Figure 3. SOHO/EIT rotated difference full-disk images with 6-hour intervals showing large-scale dimming manifestations in event *a* of the series in the coronal lines 171, 195, 284 Å (b–d) and the transition-region line 304 Å (a).

predominant meridional channels 1–11–2 and 1–4. Moreover, both dimming ribbons become elongated and their transequatorial character is more conspicuous. In comparison with events *a* and *b*, southern segment 11–2 of the eastern dimming widens, and several dimming blobs are formed along the western channel 1–4. It should be noted that dimming fragments visible clearly in this case (and somewhat fainter in other events) on the eastern half of the disk along line 14–15–16 seem to be a part of the global CME-associated disturbances originating from AR 1. As before, some fragmentary dimmings extend to the west limb and AR 6.

[14] A tendency for elongation of two transequatorial dimming channels continues in the last event *f*. It manifests itself in further development of the eastern branch 1–11–2 and, particularly, in widening and change of the orientation of the southern segment 11–2. The southern end of the western dimming channel 1–4 has reached the latitude of the southwest limb AR 10 and perhaps has a dimming branch going to this region. In turn, the main eruptive source is connected with the western over-the-limb dimming structure by narrow channel 1–5.

[15] To summarize the dimming morphology: the six events exhibit some strikingly similar dimming patterns which clearly establish the ability of the coronal structure to re-establish itself between events. The tendency towards homology on large scales suggests the existence of a coronal equilibrium established perhaps by slow and thermodynamically reversible motions, in the same sense that the loop oscillations observed by TRACE [Aschwanden *et al.*, 1999] imply the existence of an equilibrium state of the system.

[16] The EIT data are also suitable for certain analysis of multi-wave (i.e., multitemperature) manifestations of the

dimmings. We have three coronal bands: Fe IX/X (171 Å), Fe XII (195 Å), and Fe XV (284 Å) sensitive to temperatures 1.2, 1.5, and 2.0 MK, respectively, as well as a transition-region band for He II (304 Å) sensitive to 0.02–0.08 MK with a much weaker coronal component from Si XI (1 MK) [Delaboudinière *et al.*, 1995; Moses *et al.*, 1997]. In the standard mode, the corresponding images are produced every 12 min at 195 Å and only four times per day near 0100, 0700, 1300, and 1900 UT at 171, 284, and 304 Å. Fortunately, the events of our interest occurred at good times during this sequence (see Table 1). Therefore in addition to more or less detailed data at 195 Å, one can use rotated difference images with a 6-hour interval to study long-living dimmings simultaneously in the four EUV bands [Chertok and Grechnev, 2003b]. An analysis of these images (also presented at the Web site indicated above) reveals that the four-line manifestations of dimmings are more or less similar for all of six events. As an example, we demonstrate here the event *a* (Figure 3). In all four lines, including 195 Å, the rotated difference images shown were obtained from the heliograms at 0100 and 0700 UT. First of all, it is obvious that in this presentation the major large-scale channeled dimmings, visible in 12-min cadence images at 195 Å (Figure 2a), repeat themselves also in a 6-hour image (Figure 3c) and, moreover, have practically the same appearance in another moderate-temperature coronal line 171 Å (Figure 3b). This is true particularly for transequatorial dimming channels 1–2, 1–3–4, and 5–6. In both lines, the connection between dimmings 1–3–4 and 5–6 is more obvious, as well as the presence of a southern dimming zigzag around AR 6. It is essential that in the high-temperature coronal line 284 Å (Figure 3d), the channeled dimmings indicated are visible only partly, mainly in near areas southward and westward of the eruptive center 1. In the transition region line 304 Å (He II) (Figure 3a), these southern and western dimmings are hardly visible, but the most clear dimming patch appears in northeast surroundings of the eruptive center 1 where only small dimming branches are present in the coronal lines.

[17] Let us consider the CME-associated coronal waves. As usual, they are relatively weak, and for illustration we use 12-min running difference 195 Å images keeping in mind the remarks outlined in the first paragraph of this section. This representation distorts some of dimmings described above as well as some brightenings. As one can see from Figure 4 (and especially with corresponding movies), all of the events (except perhaps event *d*) were accompanied by similar coronal waves. In these running difference images, coronal waves are displayed as an emitting front, and dark fronts behind them mark the locations of the front at the time of the previous image. The main property of these disturbances is that they are also homologous, propagating anisotropically in the different events inside the same restricted angular sector. It is essential that whereas the main dimmings described above developed southward and westward of the eruptive center (AR 1), all the observed coronal waves propagated mainly in the northern and northeastern directions. In events *a*–*c*, *e*, *f*, fronts suggesting coronal waves (CW in Figure 4) are visible in the northern high-latitude region, and event *d* displays a faint diffuse brightening in the same region. Moreover, we note second and also similar emitting fronts

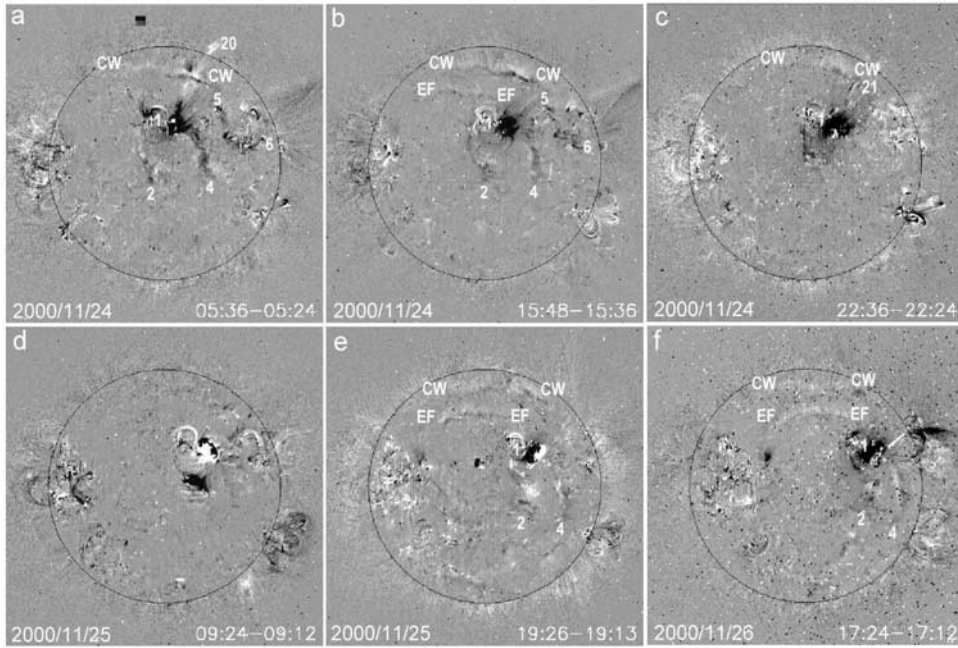


Figure 4. SOHO/EIT running difference full-disk images with 12-min intervals at 195 Å of all of six events showing homologous coronal waves (CW) and quasi-stationary emitting fronts (EF).

(EF) at least in events *b*, *e*, and *f*. A peculiarity of these emitting fronts, which can be seen with movies, is that they almost do not propagate and instead occupy more or less stationary positions on the disk [c.f. *Delannée et al.*, 2000]. It should be noted that such features as 1–2, 1–4, 5–6 in frames *a*, *b* and 1–2, 1–4 in frames *e*, *f* of Figure 4 should not be classified as coronal waves or quasi-stationary fronts, but instead reflect the evolution of the corresponding dimmings (see Figure 2).

[18] As for quantitative characteristics of the large-scale disturbances, the estimated intensity depletions in the dimmings in all four lines amount to tens of percent, and the estimated speed of the propagating coronal waves is about 100–200 km/s.

3. Discussion and Conclusions

[19] The analysis reported here demonstrates that this series of eruptive events was homologous not only in terms of the magnetic flux emergence around the preceding spot of the AR 1 and by the type of the flares and related halo CMEs, as noted in Paper I, but also from the characteristics of the accompanying large-scale activity displayed by SOHO/EIT data. First, in all six events, the CME-associated 195 Å dimmings are strongly anisotropic and can be observed in the form of analogous narrow and long channels (including transequatorial ones) extending throughout a large part of the disk southward and westward of AR 1. Moreover, this characteristic pattern is visible in at least three of the EIT bands, namely the coronal ones. Second, practically all of the events were accompanied by similar, also anisotropic coronal waves that, in contrast to dimmings, propagated northward and northeastward of AR 1 in the same restricted angular sector. It means that in these events, not only AR 1 and its nearest outskirts, but also

large-scale structures and areas were involved in the CME disturbances.

[20] Dimmings are thought to originate as a result of strong reconfigurations (the opening) of magnetic structures, identified with CMEs, and the evacuation of the plasma from them [e.g., *Hudson and Webb*, 1997; *Thompson et al.*, 1998; *Zarro et al.*, 1999; *Gopalswamy and Thompson*, 2000; *Hudson and Cliver*, 2001]. Channeled dimmings appear to be typical for the complicated solar magnetosphere near the cycle maximum [*Chertok and Grechnev*, 2002, 2003a] unlike more or less symmetrical dimmings that are observed under conditions of the relatively simple magnetosphere, for example, at the ascending phase of the cycle [*Thompson et al.*, 1998; *Gopalswamy and Thompson*, 2000]. The extended channeled dimmings superficially resemble the disappearing transequatorial interconnecting loops described by *Khan and Hudson* [2000], which also reveal homology and association with flares and CMEs. In our cases, though, the observed dimmings outline mainly the footpoints and some loop-like branches of the southward arcade as well as some interconnecting structures between the eruptive center AR 1 and western AR 6. These features erupt and reform again and again in the course of the successive CMEs. The observed location and configuration of the main CME bodies in the LASCO/C2 sky-plane images (see Figure 1 in Paper 1) appear to meet this suggestion: the brighter parts of all of the CMEs tend to be confined within a large sector of the west limb. The fact that these dimming features repeat themselves between adjacent CMEs means that the corresponding magnetic structures have time to relax and to restore their emission (i.e., density and temperature) on a time scale of several hours.

[21] The analysis of rotated difference images in four EIT lines with 6-hour intervals reveals some additional proper-

ties of the dimmings. In each event we find closely analogous large-scale channeled dimmings in the two moderate-temperature coronal bands (171 and 195 Å), while in the high-temperature band (284 Å) these dimmings are visible only partly, nearer to the eruptive center. It appears from this that not only opening of the magnetic fields, but also some temperature effects can play a role in formation of EIT dimmings. Another result of the multi-band analysis is that some dimmings are present also in the transition region line He II 304 Å and do not always coincide with coronal dimmings. Therefore the dimming process (due either to the opening of the field lines, or to temperature variations) affects not only the corona but also, to a certain extent, the transition region. Such a situation appears to be a general characteristic of dimmings initiated by large CMEs [Chertok and Grechnev, 2003b].

[22] The recurring and analogous asymmetry of coronal waves in the observed events agrees with the known feature that Moreton waves [Moreton, 1961] (the chromospheric counterparts of coronal blast waves) tend to avoid strong magnetic fields, particularly ARs [see Uchida *et al.*, 1973; Thompson *et al.*, 1999; Ofman and Thompson, 2002]. In our events, an extended zone northward and northeastward of the eruptive center and right up to the northern polar region was free from any substantial magnetic features (Figure 1). This appears to be a reason why all coronal waves propagated just through this sector of the low corona, i.e., in the direction opposite to the observed dimmings. Note however that the events studied by Khan and Hudson [2000] had the opposite behavior, with fast waves propagating into the dimming region and towards an associated active region.

[23] Thompson *et al.* [1998] found that (typically slower) coronal waves can be stopped by a polar CH resulting in prolonged brightening in a fixed location along a CH boundary. In our case, neither soft X-ray nor 284 Å images indicate the presence of a northern polar CH (Figure 1). Nevertheless, besides propagating coronal waves, similar quasi-stationary emitting fronts are observed in at least three of the events. Delannée [2000] argued that such quasi-stationary fronts could be related to quasi-separatrix layers [Démoulin *et al.*, 1996] originating from the interaction of large-scale magnetic fluxes particularly between ARs. It is not clear in what extent this explanation can be applied to our cases, because the observed quasi-stationary fronts were located in a relatively quiet high-latitude region.

[24] The features we have described allow us to conclude that the CME-associated coronal disturbances were homologous and large-scale in nature. The rapid reformation of these coronal structures suggests that some of the dimmings may not have resulted from the actual opening of coronal field into the solar wind. The opening of the field would imply an irreversible process. Instead the coronal restructurings we observe may have corresponded to partial eruptions, in which a homologous contraction followed the event-related expansion of the structure. The filament arcade south of the flaring active region provides a good example of this. We suggest that the mechanism for these reversible changes involves the transient perturbation of the global coronal force structure, which in equilibrium requires a balance of the magnetic forces, the solar wind, and gravity. This perturbation results from the magnetic restructuring restricted to the domains of the flare and CME. The

occurrence of homologous distortions of the large-scale coronal field therefore suggests the presence of a robust equilibrium in these regions. We note that TRACE loop oscillations [Aschwanden *et al.*, 1999] also sometimes seem to reflect the existence of a stable equilibrium state in regions near sites of sudden activity.

[25] **Acknowledgments.** The authors thank the SOHO/EIT team members for images used in this study. SOHO is a mission of international cooperation between ESA and NASA. The work of I. C. and V. G. was supported by the Russian Foundation of Basic Research under grants 03-02-16049 and 03-02-16591 and the Ministry of Industry and Science under grants 477.2003.2 and 1445.2003.2. The work of H. S. H. was supported by the DoD MURI grant “Understanding Magnetic Eruptions on the Sun and their Interplanetary Consequences,” and that of N. V. N. by NASA under grant NAS8-40108.

[26] Shadia Rifai Habbal thanks Takeo Kosugi and Simon P. Plumkett for their assistance in evaluating this paper.

References

- Aschwanden, M. J., L. Fletcher, C. J. Schrijver, and D. Alexander (1999), Coronal loop oscillations observed with the Transition Region and Coronal Explorer, *Astrophys. J.*, 520, 880.
- Breuckner, G. E., et al. (1995), The Large Angle Spectroscopic Coronagraph (LASCO), *Solar Phys.*, 162, 357–402.
- Chertok, I. M., and V. V. Grechnev (2002), SOHO/EIT data on global canalized dimmings in halo CME events, in *Proceedings of the 10th European Solar Physics Meeting, ESA SP-506*, vol. 1, pp. 117–120, Eur. Space Agency, Paris.
- Chertok, I. M., and V. V. Grechnev (2003a), Solar large-scale channeled dimmings produced by coronal mass ejections, *Astron. Rep.*, 47, 139–150.
- Chertok, I. M., and V. V. Grechnev (2003b), Large-scale dimmings caused by coronal mass ejections at the Sun according to SOHO/EIT data in four EUV lines, *Astron. Rep.*, 47, 934–945.
- Delaboudinière, J.-P., et al. (1995), EIT: Extreme-Ultraviolet Imaging Telescope for the SOHO Mission, *Solar Phys.*, 162, 291–312.
- Delannée, C. (2000), Another view of the EIT wave phenomenon, *Astrophys. J.*, 546, 512–523.
- Démoulin, P., J. C. Henoux, E. R. Priest, and C. H. Mandrini (1996), Quasi-separatrix layers in solar flares. I. Method, *Astron. Astrophys.*, 308, 643–655.
- Domingo, V., B. Fleck, and A. I. Poland (1995), The SOHO mission: An overview, *Solar Phys.*, 162, 1–37.
- Gopalswamy, N., and B. J. Thompson (2000), Early life of coronal mass ejections, *J. Atmos. Sol. Terr. Phys.*, 62, 1457–1469.
- Handy, B. N., et al. (1999), The Transition Region and Coronal Explorer, *Solar Phys.*, 187, 229–260.
- Howard, R. A., D. J. Michels, N. A. Sheeley Jr., and M. J. Koomen (1982), The observation of a coronal transient directed at earth, *Astrophys. J.*, 263, L101–L104.
- Hudson, H. S., and E. W. Cliver (2001), Observing CMEs without coronagraphs, *J. Geophys. Res.*, 106, 25,199–25,214.
- Hudson, H. S., and D. F. Webb (1997), Soft X-ray signatures of coronal mass ejections, in *Coronal Mass Ejections, Geophys. Monogr. Ser.*, vol. 99, edited by N. Crooker, J. Joselyn, and J. Feynman, pp. 27–38, AGU, Washington, D. C.
- Kahler, S. W. (1977), The morphological and statistical properties of solar X-ray events with long decay times, *Astrophys. J.*, 214, 891–897.
- Khan, J. I., and H. S. Hudson (2000), Homologous sudden disappearances of transequatorial interconnecting loops in solar corona, *Geophys. Res. Lett.*, 27, 1083–1086.
- Kosugi, T., et al. (1991), The Hard X-ray Telescope (HXR) for the Solar-A mission, *Solar Phys.*, 136, 17–36.
- Moreton, G. F. (1961), Fast-moving disturbances on the Sun, *Sky Telescope*, 21, 145.
- Moses, D., et al. (1997), EIT observations of the Extreme Ultraviolet Sun, *Solar Phys.*, 175, 571–599.
- Nitta, N. V., and H. S. Hudson (2001), Recurrent flare/CME events from an emerging flux region, *Geophys. Res. Lett.*, 28, 3801–3804.
- Ofman, L., and B. J. Thompson (2002), Interaction of EIT waves with coronal active regions, *Astrophys. J.*, 574, 440–452.
- Ranns, N. D. R., L. K. Harra, S. A. Matthews, and J. L. Culhane (2000), Emerging flux as a driver for homologous flares, *Astron. Astrophys.*, 364, 859.
- Scherrer, P. H., et al. (1995), The solar oscillation investigation - Michelson Doppler Imager, *Solar Phys.*, 162, 129–188.

- Thompson, B. J., et al. (1998), SOHO/EIT observations of an Earth-directed coronal mass ejections on May 12, 1997, *Geophys. Res. Lett.*, 25, 2465–2468.
- Thompson, B. J., et al. (1999), SOHO/EIT observations of the 1997 April 7 coronal transient: Possible evidence of coronal Moreton waves, *Astrophys. J.*, 517, L151–L154.
- Tsuneta, S., et al. (1991), The Soft X-ray Telescope (SXR) for the Solar-A mission, *Solar Phys.*, 136, 37–67.
- Uchida, Y., M. D. Altschuler, and G. Newkirk Jr. (1973), Flare-produced coronal MHD fast-mode wavefronts and Moreton's wave phenomenon, *Solar Phys.*, 28, 495–516.
- Wang, H., P. Gallagher, V. Yurchyshyn, G. Yang, and P. R. Goode (2002), Core and large-scale structure of the 2000 November 24 X-class flare and coronal mass ejection, *Astrophys. J.*, 569, 1026–1031.
- Zarro, D. M., A. C. Sterling, B. J. Thompson, H. S. Hudson, and N. Nitta (1999), SOHO EIT observations of extreme-ultraviolet “dimmings” associated with a halo coronal mass ejections, *Astrophys. J.*, 520, L139–L142.
-
- I. M. Chertok, IZMIRAN, Troitsk, Moscow Region, 142190, Russia.
(ichertok@izmiran.troitsk.ru)
- V. V. Grechnev, ISTP SD RAS, Irkutsk, 664033, Russia. (grechnev@iszf.irk.ru)
- H. S. Hudson, Space Sciences Laboratory, University of California, Berkeley, CA 94720, USA. (hhudson@ssl.berkeley.edu)
- N. V. Nitta, Lockheed Martin Solar and Astrophysics Laboratory, Dept/L9-41, D/252, 3251 Hanover Street, Palo Alto, CA 94304, USA.
(nitta@lmsal.com)